


# Universality of continuous phase transitions on random Voronoi graphs

Manuel Schrauth  and Jefferson S. E. Portela 

*Institute of Theoretical Physics and Astrophysics, University of Würzburg, 97074 Würzburg, Germany*

 (Received 2 August 2019; revised manuscript received 30 October 2019; published 16 December 2019)

The Voronoi construction is ubiquitous across the natural sciences and engineering. In statistical mechanics, however, only its dual, the Delaunay triangulation, has been considered in the investigation of critical phenomena. In this paper we set to fill this gap by studying three prominent systems of classical statistical mechanics, the equilibrium spin-1/2 Ising model, the nonequilibrium contact process, and the conserved stochastic sandpile model on two-dimensional random Voronoi graphs. Particular motivation comes from the fact that these graphs have vertices of constant coordination number, making it possible to isolate topological effects of quenched disorder from node-intrinsic coordination number disorder. Using large-scale numerical simulations and finite-size scaling techniques, we are able to demonstrate that all three systems belong to their respective clean universality classes. Therefore, quenched disorder introduced by the randomness of the lattice is irrelevant and does not influence the character of the phase transitions. We report the critical points to considerable precision and, for the Ising model, also the first correction-to-scaling exponent.

DOI: [10.1103/PhysRevE.100.062118](https://doi.org/10.1103/PhysRevE.100.062118)

## I. INTRODUCTION

Many location optimization problems can be approached through area-of-influence considerations. A simple example is that of several fire stations distributed over a large city. Rather naturally, the area of responsibility attributed to a particular fire station should include those buildings which lie closer to it than to any other station. The resulting tessellation of the city map defines the so-called Voronoi graph (VG). In Fig. 1, the red dots would denote fire stations, with the corresponding VG being depicted in green. Due to its conceptual simplicity, Voronoi constructions can be found in a large number of applications spanning all fields of physical sciences, including climate modeling [1,2], crystal structure [3], cosmology [4,5], microbiology [6], and growth processes [7], as well as optimization problems [8], game theory [9–11], artificial intelligence [12,13] and, recently, also in the field of machine learning [14], among others. Moreover, numerous generalizations have been defined, such as weighted graphs, and Voronoi graphs on spherical and general curved surfaces [15,16], as well as for fuzzy point sets [17] or metrics other than Euclidean [18].

In this paper, the VG is used as a discrete spatial lattice on top of which the physical system is evolved. During the evolution the lattice remains static, i.e., we consider *quenched* disorder [19]. As the graph is constructed from a randomly distributed set of points it is said to present *topological* randomness, as opposed to conventional disorder, as, e.g., in the case of randomly diluted regular structures.

Quenched disorder in general constitutes a relevant perturbation on the phase transition, i.e., it may change the universal properties of the model [20]. The first major result on disorder relevance was brought forward by Harris in 1974 [21], who argued that disorder is relevant when  $d\nu < 2$ , where  $d$  is the dimension of the system and  $\nu$  denotes the correlation length exponent. Using Harris' criterion, numer-

ical results on two-dimensional diluted regular lattices can be entirely explained, including the rise of nonconventional activated scaling and strong Griffiths effects for the contact process (CP) [22–24], as well as ambiguities related to strong logarithmic corrections for the Ising model [25–34], which represents the marginal case, as in two dimensions  $\nu = 1$ . Despite its success in describing the effects of uncorrelated disorder, the Harris criterion fails to explain certain results for the Ising model and CP on two-dimensional Delaunay triangulations [35–42], where both systems retain their clean universal properties. In order to explain these observations, a generalization has been proposed by Barghathi and Vojta [43] (based on earlier arguments of Luck [44]), which attributes the nonrelevance to strong spatial anticorrelations in the coordination numbers of the lattice nodes. Also for this improved criterion, however, violations have been found [45]. Moreover, as the argument specifically relies on fluctuations in the local coordination numbers, this criterion is silent about random structures with *constant* coordination number, such as the VG, where each site has exactly three neighbors (compare Fig. 1).

Although the Harris criterion is commonly applied to both equilibrium and nonequilibrium transitions, recent studies of the Manna universality class [46] raised doubt about whether the criterion is generally applicable in the latter case. Namely, in a series of studies [47–49], Monte Carlo simulations showed that both discrete and continuum realizations of the Manna class display unchanged critical behavior when strong disorder in the form of random impurities is introduced. Since, due to a correlation length exponent of  $\nu \approx 0.8$ , Harris' inequality predicts disorder to be relevant in this case, these unexpected results remain to be explained.

In summary, finding a complete criterion for the influence of (topological) disorder on continuous phase transitions still remains an unsolved puzzle, to which the study of critical phenomena on constant coordination lattices can provide valuable

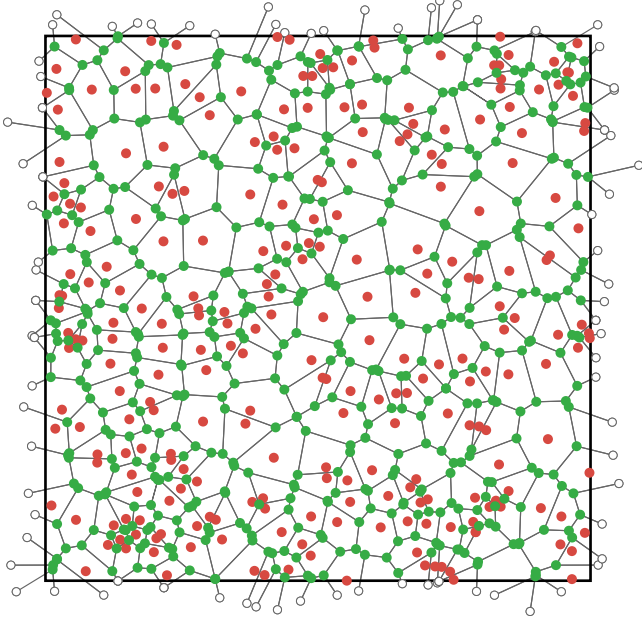


FIG. 1. Voronoi graph (green) with periodic boundaries, generated from a set of a Poissonian random points (red).

new pieces. One such puzzle piece is given in the current work, where numerical simulations of the Ising model, the CP, and the conserved stochastic sandpile model (CSSM) on two-dimensional VGs show clean universal behavior, revealing the perturbations by quenched topological randomness to be irrelevant for these systems.

The paper is organized as follows. In Sec. II we review the construction rules of the VG. In Secs. III, IV, and V we present and analyze numerical simulations of the Ising model, the CP and the CSSM, respectively. Finally, in Sec. VI we present our concluding remarks.

## II. VORONOI GRAPH

The Voronoi diagram is a partition of the plane into cells, generated by a set of points  $P = \{p_1, p_2, \dots, p_N\}$  such that for each cell corresponding to the point  $p_i$ , every point  $q$  in that cell is closer to  $p_i$  than to any other point  $p_j$ , i.e.,  $d(q, p_i) < d(q, p_j) \forall p_j \neq p_i$ . It is the geometric dual of the Delaunay triangulation, which can be constructed by connecting points corresponding to adjacent Voronoi cells. The VG is defined by taking as sites the corners of the cells and, as edges, the boundaries between the cells. Therefore the new set of points  $P' = \{p'_1, p'_2, \dots, p'_{2N}\}$  is twice as large as the original set that defined the cells. This can be easily seen from the Euler characteristic of a finite graph, which is defined as  $\chi = N - E + F$ , where  $N$ ,  $E$ , and  $F$  are the number of vertices, edges, and faces. For the periodic boundary conditions used here  $\chi = 0$  holds. In a Delaunay triangulation,  $E = 3N$  as the average coordination number is exactly  $q = 6$  and any edge is shared by two triangles. Therefore we end up with  $F = 2N$  faces in the triangulation and hence  $2N$  points in the VG due to the duality property. The location of the VG sites is given by the center of the circumcircle of the corresponding triangle in the Delaunay triangulation. A sample of a periodic VG is

shown in Fig. 1. It can be easily seen that all cells have convex shape and that every site has exactly three neighbors. This latter feature, the absence of coordination number fluctuations, constitutes a major motivation of this study. We build VGs from Delaunay triangulations, and for constructing the initial Delaunay triangulations we use the Computational Geometry Algorithms Library (CGAL) library [50].

## III. ISING MODEL

The classical Ising model [51] is defined by the Hamiltonian

$$\mathcal{H} = - \sum_{\langle i, j \rangle} J_{ij} s_i s_j + \sum_i h_i s_i, \quad s_i = \pm 1, \quad (1)$$

where  $s_i$  are discrete spins on the lattice sites,  $J_{ij}$  denotes the coupling between nearest neighbors  $\langle i, j \rangle$ , and  $h_i$  is the external field at site  $s_i$ . For equilibrium lattice models, quenched disorder can be introduced in a variety of ways. For fixed ferromagnetic coupling  $J_{ij} = J > 0$  and random external field, the system is called random field Ising model and has been investigated thoroughly over the past decades [52]. In contrast, for vanishing external field but randomly distributed (anti)ferromagnetic bonds, the system shows the behavior of a spin glass (Ref. [19] and references therein). In the present study, quenched disorder is introduced as topological randomness encoded in the implicit connectivity of the Voronoi graph. We fix all couplings to unity at vanishing external field. Sites are hence equally influenced by all of their nearest neighbors, irrespective of spatial distances. This natural choice should not imply any loss of generality since, as long as the interactions remain effectively short ranged, it is known that the properties of the phase transition are not affected. In particular, this has been shown for coupling strengths decaying exponentially with the distance in Refs. [38, 53].

For the simulation of the Ising model at criticality state-of-the-art importance-sampling Monte Carlo methods are employed, using cluster, as well as local, update algorithms. In particular, we use the algorithm proposed by Wolff [54], which significantly reduces the critical slowing down and is furthermore straightforwardly applicable to disordered lattices. Although the cluster updates preserve ergodicity, we add local Metropolis updates [55] in order to make sure that the short-wavelength modes are properly thermalized.

In the study of disordered systems, it is necessary to average physical observables over many different, independent disorder realizations of the system, also called *replicas*. The quenched averages over  $N_r$  replicas are performed at the level of (extensive) observables, rather than at the level of the partition function [19]. Denoting quenched averages as

$$[\mathcal{O}]_{\text{avg}} \equiv \frac{1}{N_r} \sum_{i=1}^{N_r} \mathcal{O}_i \quad (2)$$

and thermal averages as  $\langle \dots \rangle$ , we define magnetization, energy, and susceptibility as

$$M = [\langle |m| \rangle]_{\text{avg}}, \quad (3a)$$

$$E = [\langle e \rangle]_{\text{avg}}, \quad (3b)$$

$$\chi = N\beta[\langle m^2 \rangle - \langle |m| \rangle^2]_{\text{avg}}, \quad (3c)$$

respectively, where  $m$  and  $e$  denote the magnetization and energy per site of the individual spin configurations in thermodynamic equilibrium. Furthermore, the two-point finite-size correlation function is given by

$$\xi = \frac{1}{2 \sin(k_{\min}/2)} \sqrt{\frac{[\langle |\mathcal{F}^2(\mathbf{0})| \rangle]_{\text{avg}}}{[\langle |\mathcal{F}^2(\mathbf{k}_{\min})| \rangle]_{\text{avg}}}} - 1. \quad (4)$$

Here the Fourier transform of the magnetization is used, which is defined by

$$\mathcal{F}(\mathbf{k}) = \sum_j s_j \exp(i\mathbf{k}\mathbf{x}_j), \quad (5)$$

where  $\mathbf{x}_j$  denotes the spatial coordinate of site  $j$  and  $\mathbf{k}_{\min} = (2\pi/L, 0)$  represents the smallest nonzero wave vector in the finite lattice. The time series of the quantities  $m$ ,  $e$ , and  $\mathcal{F}^2(\mathbf{k}_{\min})$  is recorded during the Monte Carlo run, which allows to compute all relevant observables subsequently. Finally, the fourth- and sixth-order magnetic cumulant, also called Binder ratios [56], are given by

$$U_4 = \left[ 1 - \frac{\langle m^4 \rangle}{3\langle m^2 \rangle^2} \right]_{\text{avg}}, \quad U_6 = \left[ \frac{\langle m^6 \rangle}{\langle m^2 \rangle^3} \right]_{\text{avg}}. \quad (6)$$

These quantities together with the correlation length in units of the linear system size share the property of being invariant under RG transformations, i.e., they tend toward well-defined fixed point values as the system approaches the critical point. As a first step in our analysis we determine these values for  $R \in \{\xi/L, U_4, U_6\}$  as well as the eigenvalue  $\omega$  of the first irrelevant RG operator, using the quotient method [57–59]. This finite-size scaling (FSS) technique allows for great statistical accuracy and does not require a precise knowledge of the critical temperature. Specifically, the scaling functions  $R$  are evaluated at crossing points of  $\xi/L$  curves, where they are expected to scale as

$$R|_{Q_\xi=s} = R^* + a_R L^{-\omega}, \quad (7)$$

neglecting additional subleading correction terms. Here  $\omega$  is the leading correction-to-scaling exponent,  $R^*$  denotes the value of the RG-invariant scaling functions at the fixed point and the amplitudes  $a_R$  of the leading corrections depend on the respective scaling functions  $R$ . Furthermore, in Eq. (7) the quotients are defined as  $Q_O \equiv O(sL, T)/O(L, T)$ , which means that the observable  $O$ —in our case  $\xi$ —is measured at a temperature for which the correlation length in units of the lattice size is the same for the pair  $(L, sL)$ . We fix  $s = 2$ .

Using histogram reweighting techniques [60,61], the crossing points of  $\xi/L$  are determined precisely. The reweighting procedure is performed for every disorder replica individually and the curves are averaged afterward. Up to  $10^5$  disorder realizations are used for the smallest lattices and at least 4000 replicas for the largest ones. Every replica is initially prepared in a cold spin configuration and is thermalized using 1000 elementary Monte Carlo steps (EMCS). We checked for a proper thermalization by also performing simulations starting from a hot configuration, which gives identical results within numerical precision. In our update procedure, one EMCS consists of a full Metropolis lattice sweep and several single-cluster updates. Since the average cluster size  $\langle |C| \rangle$

TABLE I. Results of the simultaneous fits according to Eq. (7).

$L_{\min}$	$(\xi/L)^*$	$U_4^*$	$U_6^*$	$\omega$	$\chi^2/\text{d.o.f.}$
16	0.9078(2)	0.61067(2)	1.4563(2)	1.36(2)	12.6
18	0.9070(2)	0.61066(2)	1.4564(2)	1.43(2)	7.2
20	0.9066(3)	0.61066(2)	1.4564(2)	1.47(3)	5.8
24	0.9062(3)	0.61065(2)	1.4564(2)	1.53(4)	5.0
32	0.9058(3)	0.61065(3)	1.4563(2)	1.59(7)	4.7
40	0.9060(5)	0.61067(4)	1.4561(3)	1.50(12)	4.1
48	0.9063(7)	0.61069(5)	1.4559(4)	1.37(18)	4.5

in a  $d$ -dimensional system at criticality scales as  $L^{d-\gamma/\nu}$ , we increase the number of cluster updates with lattice size according to  $L^{0.25}$ , in order to keep the fraction of flipped spins approximately independent of the lattice size [37]. A detailed list of replica configurations and cluster steps can be found in Table II. The simulations reported in this section took about half a million CPU hours on an Intel Xeon E5-2697 v3 processor.

In order to obtain the fixed point phenomenological couplings and the correction exponent, we perform simultaneous fits of Eq. (7) for all three couplings  $\{\xi/L, U_4, U_6\}$  with joint  $\omega$  and for different  $L_{\min}$ , i.e., discarding the smallest lattices in the fits. As the quotients  $Q_O$  are naturally correlated in pairs  $(L, 2L)$ , we implement a fitting procedure that optimizes a generalized  $\chi^2$ , including the full self-covariance information, as proposed in Ref. [62]. Uncertainties for the fit parameters are obtained by bootstrap resampling methods [63,64]. The results are presented in Table I. As  $L_{\min}$  is increased, the fit results show slight systematic trends, caused by higher-order corrections. Above  $L_{\min} \approx 24$  the values saturate and the  $\chi^2/\text{degrees of freedom (d.o.f.)}$  of the fit does not improve further. We therefore use, as our final estimates, the averages for  $L_{\min} = 24, 32, 40$  and adopt a rather conservative uncertainty which includes the fluctuations among the single estimates as well as their individual uncertainties. This yields, as our final results,

$$\omega = 1.54(16) \quad (8)$$

and

$$(\xi/L)^* = 0.9060(5), \quad (9a)$$

$$U_4^* = 0.61066(3), \quad (9b)$$

$$U_6^* = 1.4563(5). \quad (9c)$$

Comparing our estimates for the critical couplings with reference values of the Ising model on a regular square lattice, which are known exactly, up to small uncertainties from numerical integration,  $(\xi/L)^* = 0.90505 \dots$ ,  $U_4^* = 0.61069 \dots$ ,  $U_6^* = 1.45565 \dots$  [65,66] we find that even though these quantities are only considered universal in a limited sense (they weakly depend on certain geometrical characteristics of the system [67–69]) they compare remarkably well, giving a first indication that the Ising model on a VG stays in the universality class of the clean model. Also our result for the correction exponent is noticeably smaller than the reference value on a square lattice,  $\omega = 2$  [70], though not particularly small in absolute numbers, which explains why

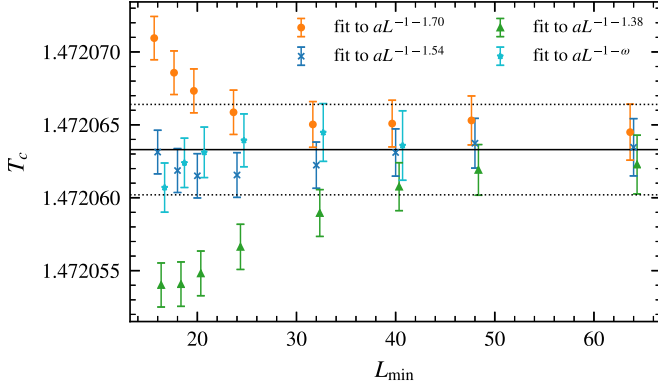


FIG. 2. Estimates for  $T_c$  from fits to Eq. (10). Some results are slightly shifted along the  $x$  axis to make them visible. The horizontal lines correspond to the final estimate  $T_c = 1.4720633(31)$ .

corrections to scaling turn out to be relatively weak in the scaling collapses described below.

Essential for computing scaling collapses is a precise knowledge of the location of the critical point, which depends on the details of the lattice structure and is therefore in general not known in advance. In the framework of quotient-FSS the critical temperature can be obtained using infinite-volume extrapolations, as the crossing points are expected to scale as [56]

$$T|_{Q_\varepsilon=s} = T_c + aL^{-\omega-1/\nu}, \quad (10)$$

where higher-order terms have been neglected as in Eq. (7), and we adopt the clean exponent  $\nu = 1$ . We perform four series of fits, where in the first three the correction exponent is fixed to our previous estimate (8), plus and minus its uncertainty, i.e.,  $\omega = 1.38, 1.54, 1.70$ . In the last series of fits  $\omega$  is treated as a free parameter. The results are displayed in Fig. 2 and listed in detail in the supplementary material [71], including  $\chi^2/\text{d.o.f.}$  values. It can be seen that for  $L_{\min} \gtrsim 40$  all four fits are compatible within their error bars. As our final estimate we take the average of the fixed- $\omega$  fits for  $L_{\min} = 64$ , obtaining

$$T_c = 1.4720633(31). \quad (11)$$

In the next step of the analysis we simulate the Ising model on Voronoi graphs of size  $L = 24, 32, \dots, 384$  for several temperatures in the vicinity of the critical point, using at least 1000 disorder replicas for every lattice size and temperature. Similarly to the precision simulations directly at criticality reported above, we start from cold configurations and perform 2500 measurements after a thermalization time of 500 EMCS. The number of cluster updates per EMCS is reduced by about a factor of 5 with respect to the values reported in Table II.

Finite-size scaling theory predicts that magnetization, susceptibility, and Binder ratio scale according to

$$[\langle m \rangle]_{\text{avg}} = L^{-\beta/\nu} f_m(x)(1 + \dots), \quad (12a)$$

$$\chi = L^{\gamma/\nu} f_\chi(x)(1 + \dots), \quad (12b)$$

$$U_4 = f_{U_4}(x)(1 + \dots), \quad (12c)$$

TABLE II. Number of disorder replicas and cluster updates per EMCS for the Ising simulations at criticality. All systems were simulated at  $T = 1.47205$ .

$L$	$N_r$	$n_{\text{Wolff}}$
16, 18, 20, 24	100 000	10
32, 36, 40, 48	100 000	12
64, 80, 96	100 000	15
128, 192, 256	35 000	17
384, 512	15 000	23
768	5000	27
1024	4000	29

where  $\beta$ ,  $\gamma$ , and  $\nu$  are critical exponents of the model and the universal scaling functions  $f$  have the argument

$$x \equiv (T - T_c)L^{1/\nu}. \quad (13)$$

These equations describe the scaling behavior to first order. Corrections of higher order are expected to become irrelevant for large system sizes. In Fig. 3 we show the scaling collapse plots, fixing all critical exponents to their exactly known

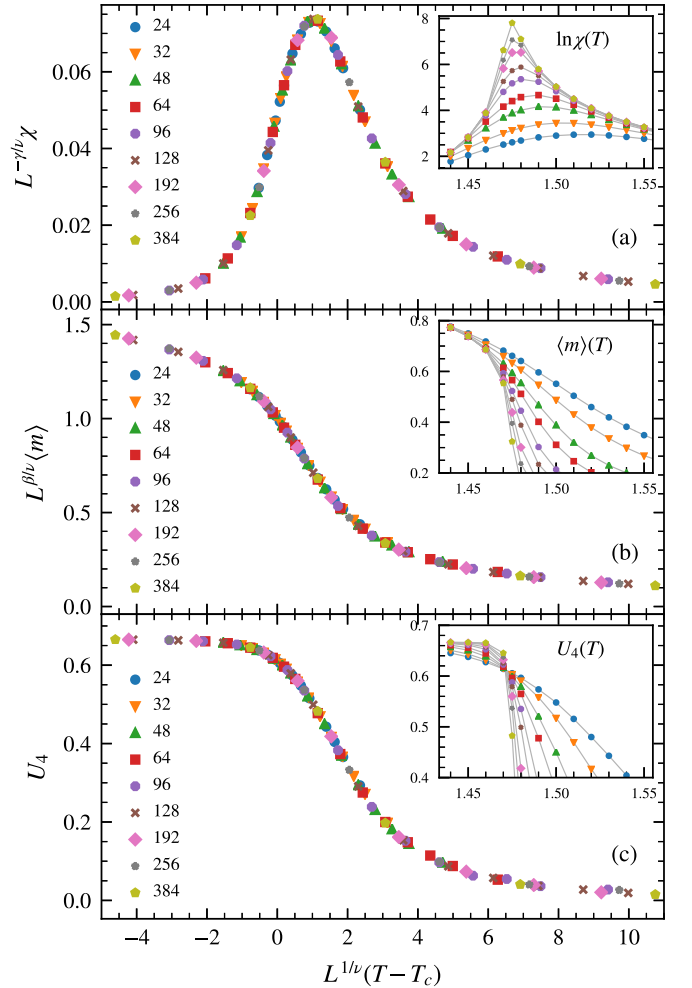


FIG. 3. Scaling collapses according to Eq. (12). The insets show the nonrescaled observables. The gray lines are only guides to the eye.



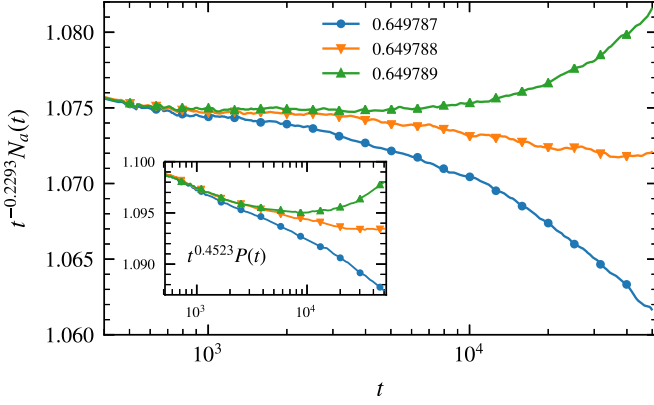


FIG. 4. Size of the active cluster for different probabilities  $p$  in seed simulations of the CP close to the critical point, rescaled by the expected universal scaling law,  $N_a(t) \sim t^\theta$ . The inset shows the survival probability of the process, rescaled according to  $P(t) \sim t^{-\delta}$ . For the critical exponents, reference values from Ref. [74] are used.

values ( $\nu = 1$ ,  $\beta = 1/8$ ,  $\gamma = 7/4$ ) and  $T_c$  to the estimate (11). As can be seen, flawless collapses for all three scaling functions are obtained even for small lattices, which shows that the Ising model on a two-dimensional (2D) random Voronoi graphs belongs to the universality class of the clean 2D Ising model.

#### IV. DIRECTED PERCOLATION

The most prominent family of nonequilibrium phase transitions arguably is the so-called directed percolation (DP) universality class. According to the Janssen-Grassberger DP conjecture, any system featuring a fluctuating phase and a unique absorbing state with scalar order parameter, no additional symmetries and only local interactions falls into this class [72,73]. On a lattice, the DP universality class is realized by certain reaction-diffusion schemes, such as the CP. In this model every site can be in either of two states, active or inactive. In the epidemic language, often used in this context, one refers to infected and recovered states. The system is evolved as a Markov process, where in each time step, one random active site is picked. With probability  $p$  it infects a random neighbor, whereas with probability  $1 - p$  the particle spontaneously recovers and is removed from the active cluster. Time is then incremented by  $1/N_a$ , where  $N_a$  denotes the size of the active cluster before the update. As soon as the system enters the so-called absorbing state where every site is inactive, the dynamics terminates.

In order to show that the CP on a random VG shows clean universal behavior we conduct numerical simulations as described in Ref. [45], in total amounting to approximately 300 000 CPU hours on an Intel Xeon E5-2697 v3 processor. As a first step, from seed simulations we determine the critical point, by rescaling the cluster size and survival probability according to their expected power law behavior,  $N_a(t) \sim t^\theta$  and  $P(t) \sim t^{-\delta}$ , where  $\theta$  and  $\delta$  denote critical exponents. In total, we use  $10^5$  independent disorder realizations of linear size  $L = 2048$  with periodic boundary conditions and performed  $10^4$  seed runs on each of them. Using reference values from Ref. [74],  $\theta = 0.2293(4)$  and  $\delta = 0.4523(10)$ , we

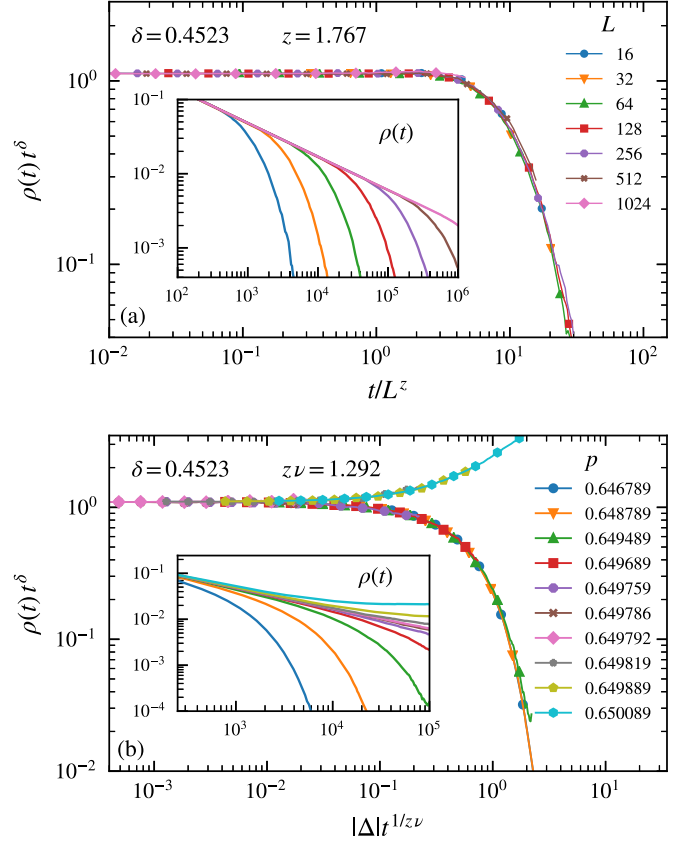


FIG. 5. Scaling collapse plots for the CP. (a) Finite-size collapse of simulations starting from a fully occupied lattice at the critical point  $p_c = 0.649788$ . (b) Data collapse in the off-critical region. The critical exponent estimates are given in the respective panels and the insets show the nonrescaled density as a function of time.

obtain the critical probability

$$p_c = 0.649788(1) \quad (14)$$

by determining the asymptotically constant curve, as shown in Fig. 4. The uncertainty is determined from curves which noticeably bend away from horizontal behavior. Note that using larger lattices and longer simulation times would not significantly increase the precision of this estimate, as the analysis is limited by the uncertainties of the reference values.

Once the critical probability is known, we perform decay simulations starting from a initially fully occupied lattice for different system sizes precisely at criticality and monitor the density  $\rho(t)$  of active sites until the system reaches the absorbing state. This allows us to obtain the exponents  $\delta$  and  $z$  via data collapses according to

$$\rho(L, t) = t^{-\delta} \tilde{\rho}(t/L^z), \quad (15)$$

where  $\tilde{\rho}$  denotes a universal scaling function. In a second set of simulations we perform decay simulations for lattices of fixed size  $L = 1024$  in the vicinity of the critical point, which gives us the exponents  $\delta$  and  $\nu_{\parallel} = zv$  by means of the relation

$$\rho(\Delta, t) = t^{-\delta} \hat{\rho}(\Delta t^{1/\nu_{\parallel}}), \quad (16)$$

where  $\Delta = p - p_c$  is the distance from criticality and  $\hat{\rho}$  a scaling function. Both scaling collapses, which turn out

flawless, are shown in Fig. 5, where we used the reference values,  $\delta = 0.4523(10)$ ,  $z = 1.7674(6)$ , and  $\nu_{\parallel} = 1.292(4)$  from Ref. [74]. In the top panel, all curves are averages over 1400 disorder realizations with five runs per realization, whereas in the bottom panel we used 250 disorder replicas and five runs per realization. The insets show the respective nonrescaled density as a function of time. This confirms the critical exponent values used and provides compelling evidence that the CP on the random VG belongs to the clean DP universality class.

### V. MANNA CLASS

A second nonequilibrium system we consider is the so-called *Manna sandpile model*. Strongly related to the celebrated concept of *self-organized criticality* (SOC), which was put forward by Bak, Tang, and Wiesenfeld (BTW) in 1987 [75,76], it can be found in a large variety of applications, such as earthquakes, forest fires, neural networks, superconductors, financial markets, and biological evolution (see Ref. [77] for a comprehensive review). In the original formulation of the BTW model, each site of a lattice harbors a number of particles, which can be interpreted as sand grains. By randomly adding new grains to the lattice, piles build up on individual sites and eventually topple. Specifically, as soon as a site exceeds a given threshold height, it becomes unstable and one grain is moved from it to each of its neighbors. If one of the neighbors thereby exceeds its threshold, then it also topples and distributes its grains. In this way a whole cascade of events might be triggered, a so-called avalanche. Certain properties of these avalanches, such as their size, area, and duration, exhibit power-law distributions. In fact, as a consequence of the slow driving mechanism (the external injection of grains), the system reaches a critical configuration without the need of fine-tuned external variables. For more details on SOC phenomena, we refer the reader to the comprehensive overview found in Ref. [78].

Based on the original BTW model, different variations have been proposed [79–82] and extensively studied. It turns out that modifying the toppling rules can change the universality class of the model [83]. In general, a distinction can be made between Abelian vs non-Abelian [84], deterministic vs stochastic, and directed vs undirected toppling rules [85]. A specific model which quickly became prominent, as an analytic solution can be obtained under certain conditions, was introduced by Manna in 1991. It presents a variation of the original BTW model with stochastic toppling rules and established the so-called Manna universality class. Due to its particularly robust and reproducible critical behavior (see Ref. [46] and references therein), this model has been studied in great detail in numerical simulations [86].

It is known that nonequilibrium systems respond strongly to boundary conditions [87–90]. Whereas in the original BTW model the boundaries of the lattice are open, allowing particles to leave the system, some variations present periodic boundary conditions and no external injection of particles, hence conserving the total number of particles. In this work we study the conserved version of the Manna model. In this model, each site can contain an unlimited number of particles  $n = 0, 1, 2, \dots$ . As long as  $n$  is below a certain threshold  $N_c$  (we

TABLE III. Simulation parameters for CSSM.  $N_r$  denotes the number of independent disorder realizations,  $M$  is the size of the history, and  $p_r$  is the associated update probability. During the first  $10^8$  time units a larger  $p_r$  (by a factor of 10) is adopted in order to efficiently erase initial states from the history.

$L$	$N_r$	$M$	$p_r \times 10^3$
32	400	4000	0.55
64	400	4000	0.20
128	400	2000	0.069
256	400	800	0.024
512	400	400	0.009
1024	192	100	0.003
2048	64	50	0.001

take  $N_c = 2$ ), a site is considered *inactive*, whereas it is *active* if  $n \geq N_c$ . The dynamics consists of toppling events where a random active site sends all of its particles to randomly chosen neighboring sites. This so-called conserved stochastic sandpile model (CSSM) no longer presents self-organized critical behavior but rather a nonequilibrium phase transition into infinitely many absorbing states (in the infinite-volume limit), controlled by the density of particles  $p = N_p/L^d$ , where  $N_p$  denotes the total number of particles in the system. In the infinite-volume limit, if  $p > p_c$ , then the systems maintains a state of steady activity, whereas for  $p < p_c$  an absorbing configuration is reached eventually.

For lattice models in the Manna universality class [91] it has been shown that the choice of initial conditions can have crucial influence on the critical behavior. For instance, correct exponents for the conserved lattice gas (CLG) models are only obtained using so-called natural initial states rather than random initial states (RIS) [92]. Furthermore, an argument raised in Ref. [93], according to which the Manna critical behavior would eventually cross over to DP universality for large times, was substantially weakened by Lee [47,94] using MC simulations of the disordered Manna model with carefully prepared initial states. The debate could finally be settled, as Dickman and da Cunha [95] showed that disorder fluctuations generated by the CSSM dynamics itself would in fact alter a DP transition, independent of the choice of initial conditions.

In this paper we perform so-called quasistationary (QS) simulations [96,97] of the two-dimensional CSSM, which should avoid ambiguities related to initial conditions altogether. We start from a RIS, where  $N_p = pL^2$  particles are randomly distributed on the lattice sites. Note that in principle  $p$  can only be tuned in steps of  $1/L^2$ . However, we are able to realize intermediate values of  $p$  by employing a stochastic linear interpolation using the disorder replicas [98]. In each time step an active site is chosen and sends each of its particles to randomly chosen neighboring sites. The time is incremented by  $1/N_a$ , where  $N_a$  is the number of active sites prior to the update, such as for the CP in Sec. IV. During the run, a history, which is a list of  $M$  system configurations is saved and periodically updated. Every time the process reaches an absorbing state, it is reset to a random configuration from its history. In order to ensure that the quasistationary state does not suffer from vestiges of the initial configuration, we run the evolution for a considerably long time of  $6 \times 10^8$  units and

take measurements after the first  $5 \times 10^8$  time units. The measured quantities are the density of active sites  $\rho$ , and the lifetime of the QS state,  $\tau$ . The latter is given by the average time between two successive visits to absorbing configurations.

We employ large lattice sizes up to  $L = 2048$  in order to reduce corrections due to subleading finite-size terms. For QS simulations of “bosonic” models, such as the CSSM, this is computationally particularly demanding, since the full configurations need to be stored, rather than only a list of active sites which would be sufficient for the CP. Moreover, the update probability  $p_r$  (per unit time) of the saved configurations represents an important tuning parameter of the QS method. As a rule of thumb it should be set such that the average residence time of a configuration in the list,  $M/p_r$ , is larger than  $\tau$  but much smaller than total duration of the run [99]. We list detailed simulation parameters in Table III.

A reliable method to obtain an accurate estimate of the critical point is to consider the ratio

$$m = [\langle \rho^2 \rangle / \langle \rho \rangle^2]_{\text{avg}}, \quad (17)$$

which is known to intersect at  $p_c$  for different lattice sizes  $L$ . In Fig. 6 the ratio is plotted for several probabilities close to criticality. Using linear interpolation in order to estimate the horizontal curve, we obtain

$$p_c = 0.721893(2) \quad (18)$$

for the critical point at an amplitude of  $m_c = 1.35(1)$ , which is compatible with the value  $m_c = 1.348(7)$ , found on a regular square lattice [42]. Once the critical point is determined, we are able to compute exponents from fits to the QS density

$$\rho_{\text{QS}} \equiv [\langle \rho \rangle]_{\text{avg}} \sim L^{-\beta/\nu}, \quad (19)$$

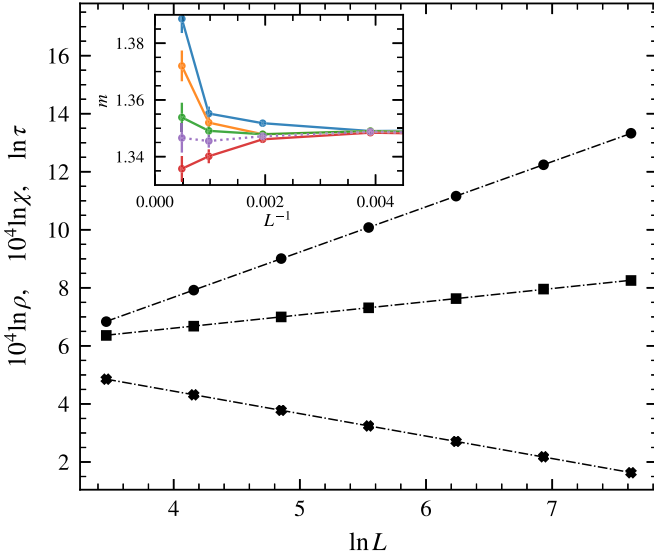


FIG. 6. Critical CSSM on a VG. Curves represent fits of the lifetime (circles), susceptibility (squares), and density of active sites (stars). The inset shows the moment ratio against the inverse lattice size for  $p = 0.721886, 0.721889, 0.721892, 0.721893, 0.721895$  from top to bottom. The curve for  $p = 0.721893$  (dashed) represents our estimate of the critical point and is interpolated linearly from its two adjacent curves. The data points connected by solid lines represent actual measurements.

TABLE IV. Critical exponent estimates from numerical Monte Carlo simulations of conserved lattice models belonging to the two-dimensional Manna universality class. The results of Lee correspond to the CSSM and the CLG. Apart from Oliveira [42], which performed their simulations on a Delaunay triangulation, all simulations used a square lattice. When no direct measurement of  $\gamma$  was available we used the relation  $\gamma = d\nu - 2\beta$  [46].

	$\beta/\nu$	$\gamma/\nu$	$z$
Dickman <i>et al.</i> [100]	0.774(3)	0.452(6)	1.572(7)
Lübeck <i>et al.</i> [101,102]	0.80(3)	0.459(25)	1.533(24)
da Cunha <i>et al.</i> [103]	0.78(1)	0.44(2)	1.510(6)
Lee [92] (CSSM)	0.785(9)	0.430(18)	1.54(2)
Lee [92] (CLG)	0.781(8)	0.438(16)	1.53(1)
Oliveira <i>et al.</i> [42]	0.78(1)	0.44(2)	1.54(2)
This work	0.773(8)	0.456(3)	1.558(23)

the average lifetime of the QS state,

$$\tau \equiv [\langle \tau \rangle]_{\text{avg}} \sim L^z, \quad (20)$$

and the susceptibility,

$$\chi \equiv L^d [\langle \rho^2 \rangle - \langle \rho \rangle^2]_{\text{avg}} \sim L^{\gamma/\nu}, \quad (21)$$

directly at criticality. We perform fits for these three equations, shown in Fig. 6, and present the corresponding results for the critical exponents in Table IV. The uncertainties of the estimates mostly stem from the uncertainty of the critical point but also include the variation due to the exclusion of some of the data points. The latter variation turns out to be very small and, significantly, there is no systematic trend visible when discarding points corresponding to ever smaller lattices from the fits. Comparing our estimates with reference values from several authors also listed in Table IV we find them to be clearly compatible, hence strongly indicating that the CSSM on the VG belongs to the clean Manna universality class.

## VI. CONCLUSION

Critical phenomena on Voronoi graphs have, to the best of our knowledge, not yet been investigated, with the focus being instead on its dual, the Delaunay triangulation. In order to correct for this omission, we conducted large-scale numerical simulations of the classical Ising model, the contact process, and the conserved Manna sandpile model on two-dimensional VGs constructed from randomly distributed sites. We establish reference values for the critical points of the three models and, for the Ising model, also obtain the first correction-to-scaling exponent. Furthermore, using finite-size scaling techniques we show that all systems display clean universal exponents at criticality, i.e., we reveal that the VG disorder is—in the sense of the RG—an irrelevant perturbation to their phase transitions. Although we only analyzed three particular models, this result has implications for other classes of transitions as well. From the RG perspective, the correlation length exponent  $\nu$  is directly related to the relevance of quenched disorder [21,39,43,44,104,105]. Hence, the phase transition of, for instance, regular (isotropic) percolation can be predicted to also remain unchanged on a

Voronoi graph, since its exponent,  $\nu = 4/3$ , is larger than for the models considered in this article. Moreover, our results are especially relevant for the search for a general disorder relevance criterion. The Voronoi graph has constant coordination number, similar to the constant coordination (CC) lattice we have recently introduced [106] and refined [107]. Studies of both the Ising and DP phase transition on the CC lattice [106,108] found disorder to be probably marginal in the Ising case and clearly *relevant* for the DP universality class. The contrast of this result with the *irrelevance* of the VG disorder shows that the absence of coordination number fluctuations is nonpredictive of disorder relevance. Thus, coordination number fluctuations do not play a central role in determining the influence of quenched topological disorder on continuous phase transitions, and a different direction, such as considering a measure of connectivity [108], should be explored in the search for a general relevance criterion.

Finally, we remark that the clean universal behavior of the Manna model on Voronoi graphs found in our simulations

can not contribute to resolving the fate of its unexpectedly stable behavior (with respect to the Harris criterion) that was reported in Refs. [47–49] for uncorrelated disorder. Instead it might be interesting to study the CSSM on other topologically disordered lattices, such as the CC lattice mentioned above, in order to obtain a clearer picture concerning the applicability of existing disorder relevance criteria [21,43,44] to nonequilibrium systems.

## ACKNOWLEDGMENTS

We thank H. Hinrichsen, F. Goth, F. P. Toldin, and R. Dickman for helpful exchanges. M.S. thanks the Studienstiftung des deutschen Volkes for financial support. This work is part of the DFG research project Hi 744/9-1. The authors gratefully acknowledge the Gauss Centre for Supercomputing e.V. for funding this project by providing computing time on the GCS Supercomputer SuperMUC at Leibniz Supercomputing Centre.

- 
- [1] T. Ringler, L. Ju, and M. Gunzburger, *Ocean Dynam.* **58**, 475 (2008).
  - [2] L. Ju, T. Ringler, and M. Gunzburger, *Numerical Techniques for Global Atmospheric Models* (Springer, Berlin, 2011), pp. 313–342.
  - [3] E. Wigner and F. Seitz, *Phys. Rev.* **43**, 804 (1933).
  - [4] R. Weygaert, V. Icke *et al.*, *Astron. Astrophys.* **213**, 1 (1989).
  - [5] M. Ramella, W. Boschin, D. Fadda, and M. Nonino, *Astron. Astrophys.* **368**, 776 (2001).
  - [6] A. Poupon, *Curr. Opin. Struct. Biol.* **14**, 233 (2004).
  - [7] W. A. Johnson and R. F. Mehl, *Trans. Metall. Soc. AIME* **135**, 416 (1939).
  - [8] A. Okabe and A. Suzuki, *Eur. J. Oper. Res.* **98**, 445 (1997).
  - [9] H.-K. Ahn, S.-W. Cheng, O. Cheong, M. Golin, and R. Van Oostrum, *Theor. Comput. Sci.* **310**, 457 (2004).
  - [10] O. Cheong, S. Har-Peled, N. Linial, and J. Matousek, *Discrete Comput. Geom.* **31**, 125 (2004).
  - [11] C. Dürr and N. K. Thang, in *European Symposium on Algorithms* (Springer, Berlin, 2007), pp. 17–28.
  - [12] K. D. Forbus, J. V. Mahoney, and K. Dill, *IEEE Intell. Syst.* **17**, 25 (2002).
  - [13] M. Gavrilova, *Generalized Voronoi Diagram: A Geometry-Based Approach to Computational Intelligence*, Studies in Computational Intelligence (Springer, Berlin, 2008).
  - [14] L. Ward, R. Liu, A. Krishna, V. I. Hegde, A. Agrawal, A. Choudhary, and C. Wolverton, *Phys. Rev. B* **96**, 024104 (2017).
  - [15] H.-S. Na, C.-N. Lee, and O. Cheong, *Comput. Geom.* **23**, 183 (2002).
  - [16] J.-D. Boissonnat, C. Wormser, and M. Yvinec, in *Effective Computational Geometry for Curves and Surfaces* (Springer, Berlin, 2006), pp. 67–116.
  - [17] M. Jooyandeh, A. Mohades, and M. Mirzakhah, *Inf. Process. Lett.* **109**, 709 (2009).
  - [18] In a more realistic fire station example one might consider using the Manhattan distance rather than the Euclidean one.
  - [19] K. Binder and A. P. Young, *Rev. Mod. Phys.* **58**, 801 (1986).
  - [20] H. Nishimori and G. Ortiz, *Elements of Phase Transitions and Critical Phenomena* (Oxford University Press, Oxford, 2010).
  - [21] A. B. Harris, *J. Phys. C: Solid State Phys.* **7**, 1671 (1974).
  - [22] T. Vojta and M. Dickson, *Phys. Rev. E* **72**, 036126 (2005).
  - [23] T. Vojta, A. Farquhar, and J. Mast, *Phys. Rev. E* **79**, 011111 (2009).
  - [24] A. H. Wada and M. J. de Oliveira, *J. Stat. Mech: Theory Exp.* (2017) 043209.
  - [25] J.-K. Kim and A. Patrascioiu, *Phys. Rev. Lett.* **72**, 2785 (1994).
  - [26] K. Ziegler, *Phys. Rev. Lett.* **73**, 3488 (1994).
  - [27] R. Kühn, *Phys. Rev. Lett.* **73**, 2268 (1994).
  - [28] V. S. Dotsenko and V. Dotsenko, *JETP Lett.* **33**, 37 (1981).
  - [29] G. Jug, *Phys. Rev. B* **27**, 4518 (1983).
  - [30] R. Shankar, *Phys. Rev. Lett.* **58**, 2466 (1987).
  - [31] J.-S. Wang, W. Selke, V. S. Dotsenko, and V. Andreichenko, *Physica A* **164**, 221 (1990).
  - [32] P. H. L. Martins and J. A. Plascak, *Phys. Rev. E* **76**, 012102 (2007).
  - [33] N. G. Fytas and P. E. Theodorakis, *Eur. Phys. J. A* **86**, 30 (2013).
  - [34] Q. Zhu, X. Wan, R. Narayanan, J. A. Hoyos, and T. Vojta, *Phys. Rev. B* **91**, 224201 (2015).
  - [35] W. Janke, M. Katoot, and R. Villanova, *Phys. Lett. B* **315**, 412 (1993).
  - [36] W. Janke, M. Katoot, and R. Villanova, *Phys. Rev. B* **49**, 9644 (1994).
  - [37] W. Janke and R. Villanova, *Phys. Rev. B* **66**, 134208 (2002).
  - [38] F. Lima, J. Moreira, J. Andrade, and U. Costa, *Physica A* **283**, 100 (2000).
  - [39] W. Janke and M. Weigel, *Phys. Rev. B* **69**, 144208 (2004).
  - [40] M. M. de Oliveira, S. G. Alves, S. C. Ferreira, and R. Dickman, *Phys. Rev. E* **78**, 031133 (2008).
  - [41] F. W. S. Lima and J. A. Plascak, *J. Phys.: Conf. Ser.* **487**, 012011 (2014).



- [42] M. M. de Oliveira, S. G. Alves, and S. C. Ferreira, *Phys. Rev. E* **93**, 012110 (2016).
- [43] H. Barghathi and T. Vojta, *Phys. Rev. Lett.* **113**, 120602 (2014).
- [44] J. Luck, *Europhys. Lett.* **24**, 359 (1993).
- [45] M. Schrauth, J. S. E. Portela, and F. Goth, *Phys. Rev. Lett.* **121**, 100601 (2018).
- [46] M. Henkel, H. Hinrichsen, S. Lübeck, and M. Pleimling, *Non-equilibrium Phase Transitions*, Vol. 1 (Springer, Berlin, 2008).
- [47] S. B. Lee, *Phys. Rev. Lett.* **110**, 159601 (2013).
- [48] S. B. Lee and J. S. Kim, *Phys. Rev. E* **87**, 032117 (2013).
- [49] S. B. Lee, *J. Stat. Mech: Theory Exp.* (2019) 053201.
- [50] N. Kruithof, *CGAL User and Reference Manual*, 4.11 ed. (CGAL Editorial Board, 2017).
- [51] E. Ising, *Z. Phys. A* **31**, 253 (1925).
- [52] T. Nattermann, *Spin Glasses and Random Fields* (World Scientific, Singapore, 1998), pp. 277–298.
- [53] F. Lima, U. Costa, M. Almeida, and J. Andrade Jr, *Eur. Phys. J. B* **17**, 111 (2000).
- [54] U. Wolff, *Phys. Rev. Lett.* **62**, 361 (1989).
- [55] N. Metropolis, A. W. Rosenbluth, M. N. Rosenbluth, A. H. Teller, and E. Teller, *J. Chem. Phys.* **21**, 1087 (1953).
- [56] K. Binder, *Z. Phys. B* **43**, 119 (1981).
- [57] H. Ballesteros, L. Fernandez, V. Martin-Mayor, and A. M. Sudupe, *Phys. Lett. B* **387**, 125 (1996).
- [58] H. Ballesteros, L. Fernández, M.-M. V., and A. Munoz, *Nucl. Phys. B* **483**, 707 (1997).
- [59] H. G. Ballesteros, L. A. Fernández, V. Martín-Mayor, A. Muñoz Sudupe, G. Parisi, and J. J. Ruiz-Lorenzo, *Phys. Rev. B* **58**, 2740 (1998).
- [60] A. M. Ferrenberg and R. H. Swendsen, *Phys. Rev. Lett.* **61**, 2635 (1988).
- [61] A. M. Ferrenberg and R. H. Swendsen, *Phys. Rev. Lett.* **63**, 1195 (1989).
- [62] A. Gordillo-Guerrero and J. J. Ruiz-Lorenzo, *J. Stat. Mech: Theory Exp.* (2007) P06014.
- [63] B. Efron and R. J. Tibshirani, *An Introduction to the Bootstrap* (Chapman & Hall, Boca Raton, FL, 1994).
- [64] We construct 250 bootstrap samples of the full data set by averaging the observables over  $N_r(L)$  randomly drawn disorder replicas rather than performing a simple average where every replica is considered exactly once. For every of those bootstrap samples the fits are performed, resulting in 250 estimates for the fit variables. Averages and standard deviations of these estimates are reported as the final results.
- [65] G. Kamieniarz and H. Blöte, *J. Phys. A* **26**, 201 (1993).
- [66] J. Salas and A. D. Sokal, *J. Stat. Phys.* **98**, 551 (2000).
- [67] W. Selke and L. N. Shchur, *J. Phys. A: Math. Gen.* **38**, L739 (2005).
- [68] W. Selke and L. N. Shchur, *Phys. Rev. E* **80**, 042104 (2009).
- [69] A. Malakis, N. G. Fytas, and G. Gülpinar, *Phys. Rev. E* **89**, 042103 (2014).
- [70] H. W. J. Blöte and M. P. M. den Nijs, *Phys. Rev. B* **37**, 1766 (1988).
- [71] See Supplemental Material at <http://link.aps.org/supplemental/10.1103/PhysRevE.100.062118> for detailed fit results of Eq. (10).
- [72] H.-K. Janssen, *Z. Phys. B* **42**, 151 (1981).
- [73] P. Grassberger, *Z. Phys. B* **47**, 365 (1982).
- [74] R. Dickman, *Phys. Rev. E* **60**, R2441 (1999).
- [75] P. Bak, C. Tang, and K. Wiesenfeld, *Phys. Rev. Lett.* **59**, 381 (1987).
- [76] P. Bak, C. Tang, and K. Wiesenfeld, *Phys. Rev. A* **38**, 364 (1988).
- [77] H. J. Jensen, *Self-organized Criticality: Emergent Complex Behavior in Physical and Biological systems* (Cambridge University Press, Cambridge, 1998), Vol. 10.
- [78] G. Pruessner, *Self-organised Criticality: Theory, Models and Characterisation* (Cambridge University Press, Cambridge, 2012).
- [79] Z. Olami, H. J. S. Feder, and K. Christensen, *Phys. Rev. Lett.* **68**, 1244 (1992).
- [80] B. Drossel and F. Schwabl, *Phys. Rev. Lett.* **69**, 1629 (1992).
- [81] P. Bak and K. Sneppen, *Phys. Rev. Lett.* **71**, 4083 (1993).
- [82] S. Manna, *J. Phys. A: Math. Gen.* **24**, L363 (1991).
- [83] A. Ben-Hur and O. Biham, *Phys. Rev. E* **53**, R1317 (1996).
- [84] A model is said to be Abelian if the configuration after the avalanche does not depend on the order in which the relaxation of the active sites was performed.
- [85] E. Milshtein, O. Biham, and S. Solomon, *Phys. Rev. E* **58**, 303 (1998).
- [86] H. N. Huynh, G. Pruessner, and L. Y. Chew, *J. Stat. Mech.: Theory Exp.* (2011) P09024.
- [87] H. Janssen, B. Schaub, and B. Schmittmann, *Z. Phys. B* **72**, 111 (1988).
- [88] K. B. Lauritsen, P. Fröjdh, and M. Howard, *Phys. Rev. Lett.* **81**, 2104 (1998).
- [89] P. Fröjdh, M. Howard, and K. B. Lauritsen, *J. Phys. A: Math. Gen.* **31**, 2311 (1998).
- [90] P. Fröjdh, M. Howard, and K. B. Lauritsen, *Int. J. Mod. Phys. B* **15**, 1761 (2001).
- [91] Apart from the CSSM, e.g., also the conserved threshold transfer process and the CLG model fall into the Manna universality class in  $d \geq 2$  spatial dimensions.
- [92] S. B. Lee, *Phys. Rev. E* **89**, 062133 (2014).
- [93] M. Basu, U. Basu, S. Bondyopadhyay, P. K. Mohanty, and H. Hinrichsen, *Phys. Rev. Lett.* **109**, 015702 (2012).
- [94] S. B. Lee, *Phys. Rev. E* **89**, 060101(R) (2014).
- [95] R. Dickman and S. D. da Cunha, *Phys. Rev. E* **92**, 020104(R) (2015).
- [96] M. M. de Oliveira and R. Dickman, *Phys. Rev. E* **71**, 016129 (2005).
- [97] R. Dickman and M. M. de Oliveira, *Physica A* **357**, 134 (2005).
- [98] For instance, consider a two-dimensional lattice of linear size  $L = 10$ . Due to the number of initially placed particles necessarily being integer,  $p$  can only be varied in steps of  $\Delta p = 1/L^2 = 0.01$ . Now say we want to realize a density given by  $p = 0.7078$ . First we distribute  $\text{floor}(pL^2)$  particles on the lattice. Then, a random number in the range  $[0, 1)$  is drawn and compared to  $p \equiv \text{mod}(pL^2, 1)$ . If  $p > p$ , then one additional particle is added. Repeating this procedure for every disorder realization we end up with, on average,  $pL^2$  particles.
- [99] We used  $p_r \approx 0.1/L^z$ , where  $z$  is the dynamic exponent.
- [100] R. Dickman, T. Tomé, and M. J. de Oliveira, *Phys. Rev. E* **66**, 016111 (2002).
- [101] S. Lübeck, *Phys. Rev. E* **66**, 046114 (2002).

- [102] S. Lübeck and P. C. Heger, [Phys. Rev. E \*\*68\*\*, 056102 \(2003\)](#).
- [103] S. D. da Cunha, L. R. da Silva, G. M. Viswanathan, and R. Dickman, [J. Stat. Mech: Theory Exp. \(2014\) P08003](#).
- [104] A. Weinrib and B. I. Halperin, [Phys. Rev. B \*\*27\*\*, 413 \(1983\)](#).
- [105] W. Kinzel, [Z. Phys. B \*\*58\*\*, 229 \(1985\)](#).
- [106] M. Schrauth, J. A. J. Richter, and J. S. E. Portela, [Phys. Rev. E \*\*97\*\*, 022144 \(2018\)](#).
- [107] M. Schrauth and J. S. E. Portela, [Phys. Rev. Res. \*\*1\*\*, 033061 \(2019\)](#).
- [108] M. Schrauth, J. S. E. Portela, and F. Goth, [arXiv:1907.05809 \(2019\)](#).